SCIENTIFIC REPORTS

OPEN

SUBJECT AREAS:
BACTERIA
ENZYMES

Received
15 August 2013

Accepted
31 October 2013

Published
18 November 2013

Correspondence and requests for materials should be addressed to P.X. (pingxu@sjtu.edu.cn)

Iron(II)-dependent dioxygenase and *N*-formylamide deformylase catalyze the reactions from 5-hydroxy-2-pyridone to maleamate

Yuxiang Yao[1], Hongzhi Tang[1], Huixue Ren[2], Hao Yu[1], Lijuan Wang[1], Wei Zhang[1], Edward J. Behrman[3] & Ping Xu[1]

[1]State Key Laboratory of Microbial Metabolism, and School of Life Sciences & Biotechnology, Shanghai Jiao Tong University, Shanghai 200240, PR China, [2]School of Municipal and Environmental Engineering, Shandong Jian Zhu University, Jinan 250101, P.R. China, [3]Department of Chemistry and Biochemistry, The Ohio State University, Columbus, Ohio 43210, USA.

5-Hydroxy-2-pyridone (2,5-DHP) is a central metabolic intermediate in catabolism of many pyridine derivatives, and has been suggested as a potential carcinogen. 2,5-DHP is frequently transformed to *N*-formylmaleamic acid (NFM) by a 2,5-DHP dioxygenase. Three hypotheses were formerly discussed for conversion of 2,5-DHP to maleamate. Based on enzymatic reactions of dioxygenase (Hpo) and *N*-formylamide deformylase (Nfo), we demonstrated that the dioxygenase does not catalyze the hydrolysis of NFM but rather that this activity is brought about by a separate deformylase. We report that the deformylase acts both on NFM and its *trans*-isomer, *N*-formylfumaramic acid (NFF), but the catalytic efficiency of Nfo for NFM is about 1,400 times greater than that for NFF. In addition, we uncover catalytic and structural characteristics of the new family that the Hpo belongs to, and support a potential 2-His-1-carboxylate motif ($HX_{52}HXD$) by three-dimensional modeling and site-directed mutagenesis. This study provides a better understanding of 2,5-DHP catabolism.

Large quantities of wastes containing the pyridine ring are produced from coal and shale oil processing, pharmaceutical, food, dye and tobacco industries, and agriculture[1,2]. They are classified as priority pollutants by USEPA (United States Environmental Protection Agency) because of their toxicity, carcinogenicity, and environmental hazards[3,4]. Their hydrophilic nature contributes to their environmental danger[5,6]. Many pyridine derivatives such as 2- and 3-hydroxypyridine, nicotinic acid, and nicotine are degraded by aerobic microorganisms to generate 5-hydroxy-2-pyridone (2,5-dihydroxypyridine, 2,5-DHP) as an intermediate (Fig. 1)[7–13]. 2,5-DHP was shown to cause DNA strand scission and suggested as a potential carcinogen[14]. 2,5-DHP is subsequently oxidized to form *N*-formylmaleamic acid (NFM) and then hydrolyzed to maleamate and formate by some *Pseudomonas* species (shown in the red oval of Fig. 1)[7,10,13]. This pathway was first shown by Behrman and Stanier in *Pseudomonas putida* N-9 (formerly known as *P. fluorescens*)[15,16].

2,5-DHP oxygenase, termed NicX or Hpo for the enzyme from *P. putida* strain KT2440 or strain S16, respectively, catalyzes the dioxygenation of 2,5-DHP[10,13]; however, it has been disputed for about 40 years whether or not 2,5-DHP dioxygenases also catalyze NFM hydrolysis[13,17–21]. Investigation of the further transformation of NFM has not been straightforward for several reasons. Gauthier and Rittenberg studied the enzymatic hydrolysis of what they thought was NFM, and they reported that the purified 2,5-DHP oxygenase had both dioxygenase and deformylase activities[18]. Behrman showed that the compound synthesized by Gauthier and Rittenberg was the *trans* isomer, *N*-formylfumaramic acid (NFF), and that both of these *N*-formylamides were rapidly hydrolyzed to the corresponding amides non-enzymatically. Maleamic acid is the next intermediate in the bacterial pathway whereas fumaramic acid is not metabolized by the cells. Further work was hampered by the lack of a convenient synthetic source of NFM, as the photochemical isomerization of NFF gives a mixture of geometric isomers[19]. Jiménez et al. prepared a homogeneous sample by cleavage of 2,5-DHP with a highly purified oxygenase (NicX), demonstrated that NicX did not catalyze the hydrolysis of NFM, and identified a separate deformylase (NicD) which did so in strain KT2440[13]. NFM formation and hydrolysis were studied in strain S16[10], but NFF was

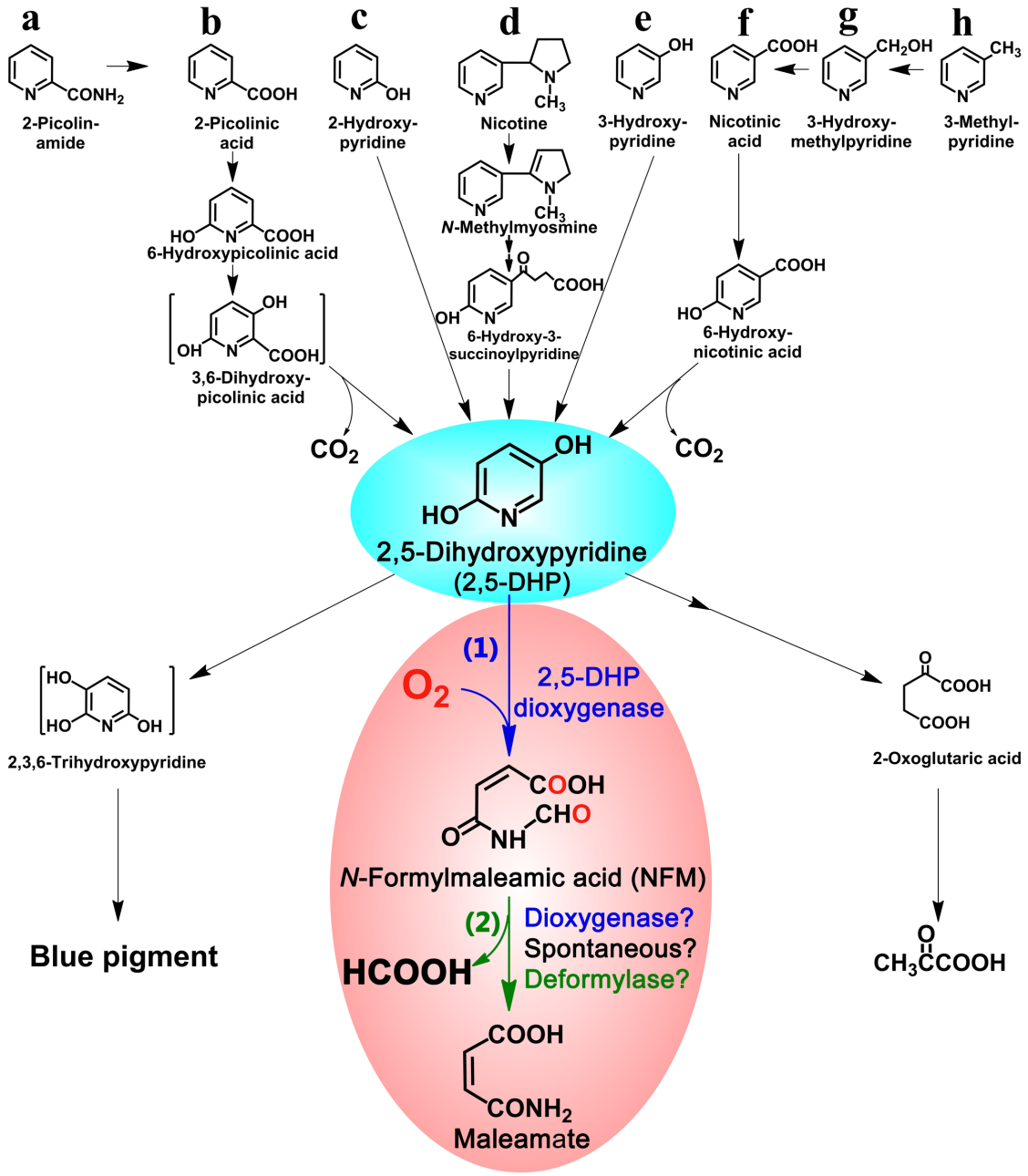

Figure 1 | Pathways that degrade pyridine derivatives through 2,5-DHP[7–13]. (a) 2-Picolinamide degrading pathway through 2,5-DHP to maleamate[7,8]; (b) 2-Picolinic acid degrading pathway through 2,5-DHP to α-oxoglutaric acid[7]; (c) 2-Hydroxypyridine degrading pathway through 2,5-DHP to blue pigment or to maleamate[7,9]; (d) Nicotine degrading pathway through 2,5-DHP to maleamate[10,11]; (e) 3-Hydroxypyridine degrading pathway through 2,5-DHP to maleamate[12]. (f) Nicotinic acid degrading pathway through 2,5-DHP to maleamate[13]; (g) 3-Hydroxy-methylpyridine degrading pathway through 2,5-DHP to maleamate[7]; (h) 3-Methylpyridine degrading pathway through 2,5-DHP to maleamate[7]; Compounds in brackets were not detected. Reactions in the red oval were studied in this paper.

mistakenly used as the deformylase substrate by following the method of Gauthier and Rittenberg[18,19]. Two syntheses of authentic NFM were reported in 2008[22].

NicX was characterized and shown to belong to a new non-heme iron(II) ring-cleavage dioxygenase family[13]. However, it is still unclear whether these properties are the general characteristics of the family or specific to NicX. The similarities and differences between the new family and other dioxygenases are also unknown. A 2-His-1-carboxylate motif is a nearly universal platform for other non-heme iron(II) dioxygenases[23], but this architecture has not yet been confirmed in the new family.

Recently, we found a 2,5-DHP dioxygenase gene (*hpo*) in a nicotine-degrading strain *P. putida* S16. Some basic catalytic characteristics of C-terminal His_6-tagged 2,5-DHP dioxygenase (His-Hpo), such as temperature effects, optimal pH, K_m value, and k_{cat} value, were characterized[10]. In this study, two 2,5-DHP dioxygenases (Hpo and NicX) and a NFM deformylase (Nfo) were heterologously expressed and purified. Using a genuine sample of NFM, we now conclude that neither NicX nor Hpo could further hydrolyze NFM to maleamate while the deformylase isolated from the nicotine-degrading organism is capable of catalyzing the hydrolysis of both NFM and NFF, but at different rates. Kinetic studies show that the catalytic efficiency of Nfo for NFM is about 1,400 times greater than that for NFF which is consistent with the semi-quantitative results of Hillenbrand, E. L. (M.S. thesis, the Ohio State University, 1980). Comparing the catalytic characteristics of Hpo and NicX, we found some similarities and

Table 1 | Hpo purification from *E. coli* BL21(DE3) harboring pET28a-*hpo*

Step	Total volume	Total protein	Total activity	Specific activity	Yield	Purification factor
	ml	mg	U	U mg^{-1}	%	Fold
Crude extract	30.2	86.0	34.4	0.40	100	1.0
Q Sepharose XL	28.5	57.7	29.8	0.52	86.5	1.3
Source 30Q	19.6	5.1	18.8	3.68	54.6	9.2
Mono Q	1.4	1.2	8.1	6.56	23.6	16.4

differences between them. Using structure prediction and site-specific mutagenesis analysis, we obtained data that support the 2-His-1-carboxylate motif of the new non-heme iron(II) dioxygenases family. The motif $HX_{52}HXD$ is different from the sequence motif of other non-heme iron(II) enzymes[23].

Results

Characterization of Hpo. 2,5-DHP dioxygenase activity was purified by following the ability to decrease the absorption of 2,5-DHP at 320 nm. After three steps of anion-exchange column chromatography, the recombinant Hpo was purified about 16-fold with an overall yield of 24% (Table 1). The molecular mass of the purified bands on sodium dodecyl sulfate-polyacrylamide gel electrophoresis (SDS-PAGE) and native polyacrylamide gel electrophoresis (native-PAGE) were approximately 38 kDa and 120 kDa, respectively, and size-exclusion chromatography analysis revealed that the mass of the purified protein as it existed in solution was about 119 ± 5 kDa, which implied a trimer (Fig. 2A, 2B, 2C). The UV-visible spectrum (data not shown) showed only a maximum at 280 nm associated with the protein, and no evidence for heme, flavin or bound ferric iron, just as was found for the dioxygenase purified by Gauthier and Rittenberg[17].

The purified enzyme was stored at −80°C in 20 mM Tris-HCl buffer (pH 7.5) containing 1 mM dithiothreitol (DTT), under which the enzyme retained more than 90% of its activity for 30 days. Contrastingly, the enzyme lost all of its activity after being stored at 0°C in 20 mM Tris-HCl buffer (pH 7.5) for 1 day. The addition of 1 mM DTT could not regenerate the activity (data not shown).

To compare the steady-state kinetic data between Hpo and NicX, NicX was purified from *E. coli* BL21(DE3) harboring plasmid pET24a-*nicX* (Table 2). The calculated K_m of Hpo for 2,5-DHP was 0.138 ± 0.013 mM, more than that of NicX (K_m = 0.074 ± 0.003 mM), and the values of V_{max} and k_{cat} of Hpo were 20.5 ± 1.0 U mg^{-1} and 12.9 ± 0.6 s^{-1}, higher than the values of NicX (2.00 ± 0.04 U mg^{-1} and 1.28 ± 0.03 s^{-1}) (Fig. S1).

O_2 consumption and ^{18}O labeling. During the first 15 s of the enzymatic reaction, the rates of decrease for O_2 and 2,5-DHP were approximately linear, 0.88 ± 0.01 μmol L^{-1} s^{-1} for O_2 and 0.90 ± 0.02 μmol L^{-1} s^{-1} for 2,5-DHP (Fig. 2D). Therefore, the ratio of O_2 used per 2,5-DHP oxidation was approximately 1 : 1.

Reactions were carried out using O-18 labeled water or oxygen, and the products were analyzed by liquid chromatography–mass spectrometry (LC-MS) to assess the source of the added oxygen. The substrate 2,5-DHP was completely transformed in the presence of O_2, while it was partially transformed in the presence of $^{18}O_2$ probably due to an insufficient $^{18}O_2$ concentration (Fig. 2E, 2F, 2G, 2H). The single product molecular ion peak detected in the presence of H_2 ^{18}O was at *m/z* 142.0152, corresponding to NFM lacking ^{18}O (theoretical *m/z* = 142.0146) (Fig. 2F, 2G). In contrast, the molecular ion peak of NFM with two ^{18}O atoms (theoretical *m/z* = 146.0231) was found for sample produced in the presence of $^{18}O_2$ (Fig. 2H). Thus the source of both oxygen atoms in the product is dioxygen, not water.

Dioxygenase substrate specificity. Many pyridine and benzene derivatives, including 2,5-DHP, 2,3-DHP, 2,4-DHP, 2,6-DHP, 2-hydroxypyridine, 3-hydroxypyridine, 4-hydroxypyridine, 2,3-pyridinedicarboxylic acid, 2,4-pyridinedicarboxylic acid, 2,5-pyridinedicarboxylic acid, 2,6-pyridinedicarboxylic acid, 3,4-pyridinedicarboxylic acid, 3,5-pyridinedicarboxylic acid, 2-picolinic acid, 4-picolinic acid, nicotinic acid, 6-hydroxynicotinic acid, pyridoxal hydrochloride, pyridoxamine hydrochloride, catechol, resorcinol, hydroquinone, pyrogallol, protocatechuate, *p*-hydroxybenzoic acid, gentisate and gallate, were tested as potential substrates of Hpo by monitoring substrates decrease and O_2 consumption. Only 2,5-DHP was oxidized, showing that the substrate specificity of Hpo is very strict.

Aminopeptidase activity of 2,5-DHP dioxygenase. The sequence of Hpo, like that of NicX, contains an aminopeptidase (AmpS)-like conserved domain according to blastp analysis[24]. Many proteins homologous to Hpo are predicted to belong to the leucine aminopeptidase (LAP) or M29 peptidase families (Fig. 3A), and such a sequence could reasonably account for the previously proposed deformylase activity of the protein. To ascertain the LAP activity of the new dioxygenase family, Hpo and NicX were used to incubate with L-Leu-*p*-nitroaniline under many conditions. No activity was detected for either sample (data not shown).

Phylogenetic and secondary structure analyses. Phylogenetic analysis showed that Hpo and NicX do not belong to any known non-heme iron(II) ring-cleavage dioxygenase family (Fig. 3B). Structure prediction indicated that the secondary structures of Hpo and NicX are similar, although the amino acid sequence identity is only 43% (Fig. 3C). The sequence alignment shows that Nfo is highly similar with those of the α/β-hydrolase-fold enzyme superfamily (Fig. S2)[13,25]. The predicted secondary structure of Nfo shows remarkable similarity to NicD (Fig. S2)[13].

Three-dimensional structure prediction and directed mutagenesis. Since the PSI-BLAST programs revealed no known 3D structure that was homologous to Hpo, the protein sequence was submitted to the mGenThreader server for fold assignment. Protein structures with significant hits were chosen as templates for further modeling (Table S1). Five models were generated for Hpo and the one with the lowest DOPE score was used for visualization (Table S2, Fig. 4A). The protein is predicted to contain two global domains. One is constituted mainly by residues from the *N*-terminal region (residues 1–126 and 173–182) and shows a Rossmann fold structure. It contains three parallel β strands (β2-β1-β3) linked to two pairs of α helices (α1–α2 and α3–α4). The other domain is mainly constituted by two layers of β sheets (β4-β5-β8-β11-β12-β16-β17-β18 and β6-β7-β9-β10-β13-β14-β1) that are flanked by α helices (α7–α8) at each side (Fig. 4A).

Despite the phylogenetic diversity of non-heme iron(II) ring-cleavage dioxygenases (Fig. 3B), each is thought to contain a 2-His-1-carboxylate facial triad for coordinating the metal ion; significantly, a similar motif was predicted for Hpo (consisting of H257, H310, and D312) (Fig. 4B). To test the significance of this motif, *E. coli* BL21(DE3) strains harboring pET28a-*hisH257R*, pET28a-*hisH310K* or pET28a-*hisD312E* plasmid were separately constructed (Table 2). The His_6-tagged variant proteins of His-H257R, His-H310K and His-D312E were purified (Fig. 4C). In these

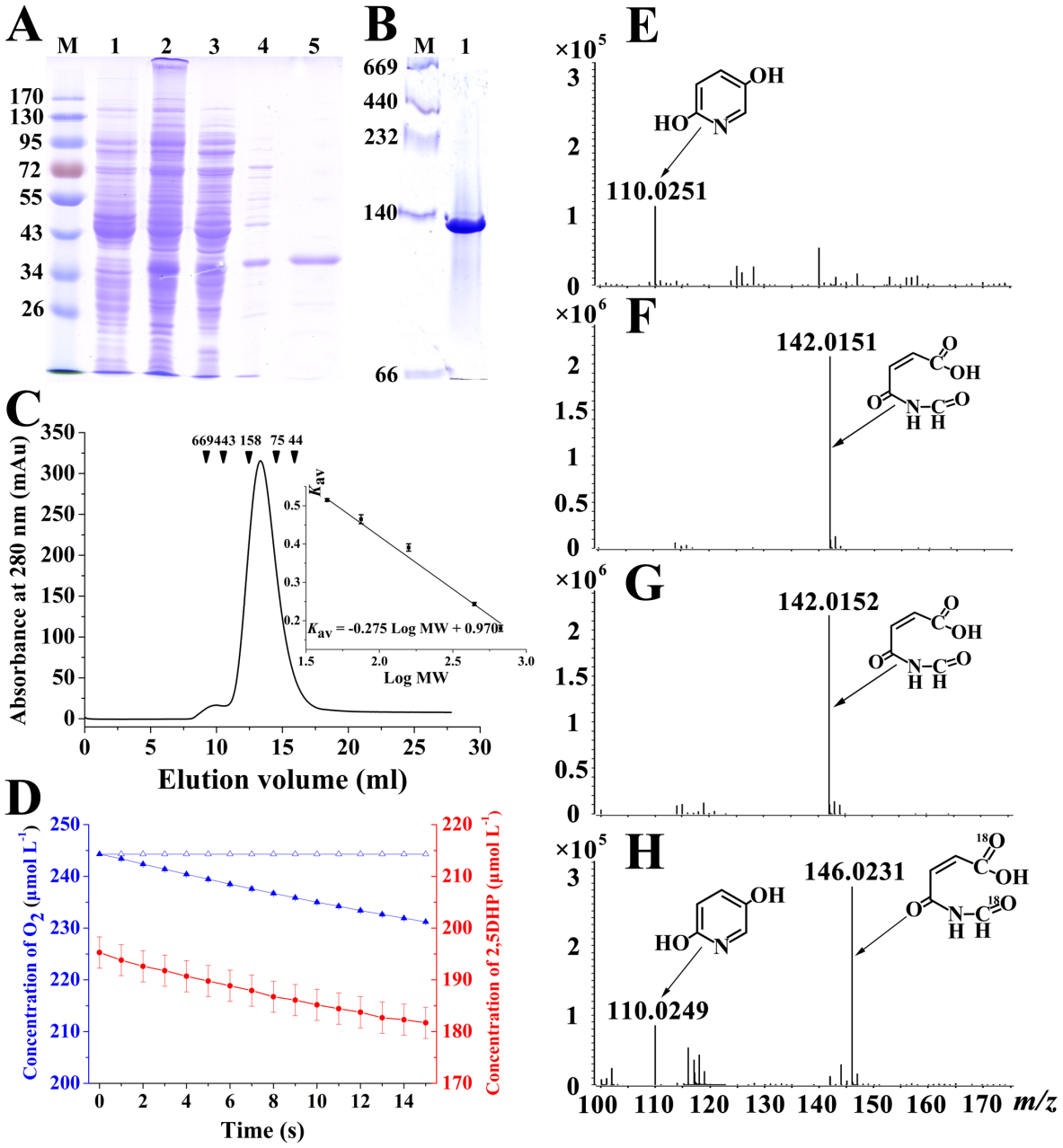

Figure 2 | Characterization of purified Hpo. (A) SDS-PAGE. M, marker proteins; 1, cell-free extracts of induced *E. coli* BL21(DE3) without plasmid; 2, cell-free extracts of induced *E. coli* BL21(DE3) harboring plasmid pET28a-*hpo*; 3, Q Sepharose XL pool; 4, Source 30Q fraction; 5, Mono Q fraction. (B) Native-PAGE of purified Hpo. M, native protein marker; 1, purified Hpo. (C) Elution profile of size-exclusion chromatography analysis of purified Hpo. Inverted triangles indicate the peak positions of standard proteins; inset is the fitted standard curve of a base-10 logarithm of the MW of the standard proteins *versus* their K_{av} values; each error bar represents standard deviation of three independent experiments. (D) O_2 consumption and substrate depletion during 2,5-DHP degradation. Each error bar represents standard deviation of three independent experiments; all samples contained 0.025 mM Fe^{2+} in 1 ml of 20 mM Tris-HCl buffer (pH 7.5) at 28°C and the following additions: 0.2 mM 2,5-DHP (open triangles), 0.2 mM 2,5-DHP and 9.6 μg Hpo (closed triangles). 2,5-DHP depletion during the reactions catalyzed by Hpo was also assayed (circles). (E), (F), (G) and (H) LC-MS analysis of ^{18}O labeling experiments. LC-MS spectrum of (E) 1 mM substrate 2,5-DHP and the product from the reaction occurring in (F) H_2O and O_2, (G) $H_2{}^{18}O$ and O_2, and (H) H_2O and $^{18}O_2$. The molecular ion peaks for 2,5-DHP, NFM and ^{18}O labeled NFM are indicated.

variants, the amino acid H257, H310 or D312 was replaced by R257, K310 or E312. The far-UV circular dichroism analysis showed that the secondary structures of the mutation variants were not changed (Fig. 4D, Table S3), and these variants lost almost all of their 2,5-DHP dioxygenase activities (Fig. 4E). This result implies that the amino acids H257, H310 and D312 are important or crucial for the activity of Hpo.

The predicted tertiary structure of Nfo shows a β-sheet enwrapped by a series of α helices (Fig. S3). The conserved catalytic triad characterized by a nucleophilic residue at the end of β5 (Ser94), an acidic residue at the end of β6 (Asp118), as well as a histidine located in a loop followed β8 (His238) was predicted (Fig. S3).

Deformylase activity. LC-MS analysis showed that both Hpo and NicX catalyze the formation of NFM from 2,5-DHP (Fig. S4). There was no significant hydrolysis of standard NFM after incubation at pH 7, 25°C, for 15 min (Fig. 5A, 5B). Neither Hpo nor NicX promoted the process (Fig. 5B, 5C, 5D), while Nfo catalyzed the process

Table 2 | Primers used for amplification and mutagenesis

Primer	Sequence (5′-3′)	Use	Recombinant plasmid
hishpo-f	5′aggcc**atgg**accatgtgagttttaccgagat3′	Amplifying the 1043-bp fragment containing *hpo*, which was digested with NcoI/XhoI and cloned into pET28a	pET28a-*hishpo*
hishpo-r	5′cggctcgag**cctttgcactagctgaatttct**3′		
hpo-f	Hishpo-f	Amplifying the 1049-bp fragment containing *hpo*, which was digested with NcoI/XhoI and cloned into pET28a	pET28a-*hpo*
hpo-r	5′cggctcgagcta**ctacctttgcactagctgaatt**3′		
hpo-H257R-f	5′**aatgagtc*g*tgtaggctggggaa**3′	Mutagenesis to obtain the *hpoH257R* mutant, which was digested with NcoI/XhoI and cloned into pET28a	pET28a-*hisH257R*
hpo-H257R-r	5′**cctttaccacggggatcatta**3′		
hpo-H310K-f	5′**ccgcctgt*a*a*a*cttgatattcc**3′	Mutagenesis to obtain the *hpoH310K* mutant, which was digested with NcoI/XhoI and cloned into pET28a	pET28a-*hisH310K*
hpo-H310K-r	5′**tatcattcgatccgccaagctc**3′		
hpo-D312E-f	5′**gcctgtcatcttga*a*attccaatgcg**3′	Mutagenesis to obtain the *hpoD312E* mutant, which was digested with NcoI/XhoI and cloned into pET28a	pET28a-*hisD312E*
hpo-D312E-r	5′**ggtatcattcgatccgccaagctcat**3′		
nicX-f	5′agtcat**atg**ccggtgagcaatgcacaa3′	Amplifying the 1065-bp fragment containing *nicX*, which was digested with NdeI/HindIII and cloned into pET24a	pET24a-*nicX*
nicX-r	5′tataagctt**tcgcgctcgcgactcct**3′		

Bold front, the native gene sequence; Italic front, the site of directed mutation; ccatgg, NcoI site; ctcgag, XhoI site; catatg, NdeI site; aagctt, HindIII site.

completely (Fig. 5E, Fig. S5). Similar results were obtained using NFF as a substrate (Fig. 5F, 5G, 5H, 5I, 5J). However, kinetic studies showed that Nfo catalyzed the hydrolysis of NFM much faster (Fig. 6). The calculated K_m, V_{max} and k_{cat} for NFM are 0.94 ± 0.06 mM, 1,106 ± 19 U mg^{-1} and 542 ± 9 s^{-1}, while these values for NFF are 5.83 ± 0.46 mM, 4.8 ± 0.3 U mg^{-1} and 2.4 ± 0.1 s^{-1}, respectively (Fig. 6). According to these results, we can deduce that 2,5-DHP dioxygenases (Hpo and NicX) have no ability to catalyze NFM hydrolysis even if it is formed by 2,5-DHP reaction with O_2. NFM hydrolysis is catalyzed by NFM deformylase, which can also catalyze NFF hydrolysis but at a reduced rate.

Discussion

The mechanism of NFM deformylation has been in dispute. Gauthier and Rittenberg deduced that it was catalyzed by 2,5-DHP oxygenase[18], while Behrman showed that the spontaneous hydrolysis of NFM was undoubtedly important under the conditions that Gauthier and Rittenberg used[18,19]. Jiménez and coworkers found a NFM deformylase activity[13]. In our studies, we found that 2,5-DHP dioxygenases Hpo and NicX catalyze 2,5-DHP ring-cleavage to generate NFM (Fig. S4), but neither enzyme could catalyze NFM deformylation (Fig. 5C, 5D). Although NFM does hydrolyze spontaneously (Fig. 5B)[19], it occurs much more slowly than the reaction catalyzed by Nfo (Fig. 5E). These findings are in good agreement with the results of Jiménez et al.[13]. Interestingly, hydrolysis of the synthetic *trans*-isomer, NFF, can also be catalyzed by Nfo and much faster than the nonenzymic hydrolysis (Fig. 5F, 5G, 5J, Fig. 6). Kinetic studies suggested that the apparent affinity of Nfo for NFM is about 6 times greater than for NFF affinity, and the catalytic efficiency for NFM is about 1,400 times larger than that for NFF (Fig. 6).

Sequence alignment and phylogenetic analysis indicates that Hpo is the second member of a new ring-cleavage dioxygenase family, whose founding member is NicX[13]. The predicted secondary structures and 3D models of the two members of the new ring-cleavage dioxygenase family are similar. They are both predicted to contain two anti-parallel β sheets (β18-β17-β16-β4-β5-β8-β11-β12 and β6-β7-β13-β14-β15-β9-β10 in Hpo, β21-β20-β19-β5-β6-β11-β14-β15 and β7-β10-β16-β17-β18-β12-β13 in NicX) flanked by α helices (α6 and α7 in Hpo, α7 and α8 in NicX) at each side of the C terminal domain (Fig. 3C, Fig. 4A)[13]. These similarities are probably the reasons for the similar properties of this new family. Hpo is a trimer in solution (Fig. 2A, 2B, 2C) and NicX is a hexameric assembly composed of 2 cyclic trimers[26] suggesting a sort of "trimer-module" is conserved in both NicX and Hpo. Hpo and NicX catalyze 5,6-dioxygenation reactions that convert 1 mole of 2,5-DHP to NFM consuming 1 mole O_2; are unstable at 0°C without DTT; are totally inhibited by metal-chelators or oxidants; depend on iron(II) and exhibit strict substrate specificity for 2,5-DHP[13]. Although AmpS-like conserved domains are present in each protein, neither Hpo nor NicX has LAP activity.

Some differences exist between the two dioxygenases. Identities of the amino acid sequences between the two dioxygenases are only 43%. These may lead to higher efficient binding pockets of Hpo than those of NicX, which may cause their differences in kinetics: the apparent affinity of Hpo for 2,5-DHP is less than that of NicX while the catalytic efficiency of Hpo is 5 times greater than that of NicX (Fig. S1). The predicted 3D structures of NicX and of Hpo were some different. The *N*-terminal domain of NicX was predicted to contain six β strands (β2-β1-β3-β4-β9-β8) flanked by six α helices (α1-α2-α3-α4-α5-α6)[13], while the *N*-terminal domain of Hpo was predicted to contain only 3 β strands (β2-β1-β3) and 5 α helices, with 3 at one side (α1, α2, and α5) and another 2 (α3 and α4) at the other side (Fig. 4A).

The 2-His-1-carboxylate metal-binding motif, consisting of two His residues and an Asp/Glu residue, that exists in a wide array of non-heme iron(II) enzymes[23] is also predicted to be present in Hpo (composed of H257, H310, D312). Site-directed mutations led to variants at these positions, suggesting that they were all necessary for their activity (Fig. 4D, 4E, Table S3). Different from other known non-heme iron(II) ring-cleavage dioxygenases, the carboxylate donor of the 2-His-1-carboxylate motif in the new family might be an Asp residue rather than Glu. The D312 residue cannot be replaced by E312 residue in Hpo (Fig. 4E). The sequence of 2-His-1-carboxylate motif in the new family ($HX_{52}HXD$) is distinct from other non-heme iron(II) enzymes[23].

Sequence alignment and structure predictions reveal that Nfo is a member of α/β-hydrolase-fold superfamily which NicD belongs to (Fig. S2, Fig. S3)[13,25]. The residues forming the catalytic triads of Nfo (S94, D118 and H238) and NicD (S101, D125 and H245) were proposed to be the same (Fig. S2, Fig. S3)[13]. Although Jiménez et al. proved the indispensability of S101, D125 and H245 for the activity of NicD with site-directed mutagenesis[13], many things about structures and catalytic mechanisms of Nfo and NicD are still unknown. For example, it should be clarified why Nfo and NicD have deformylase activity while other α/β-hydrolases do not when even the catalytic triads are conserved[13,25]. An x-ray structure of Nfo

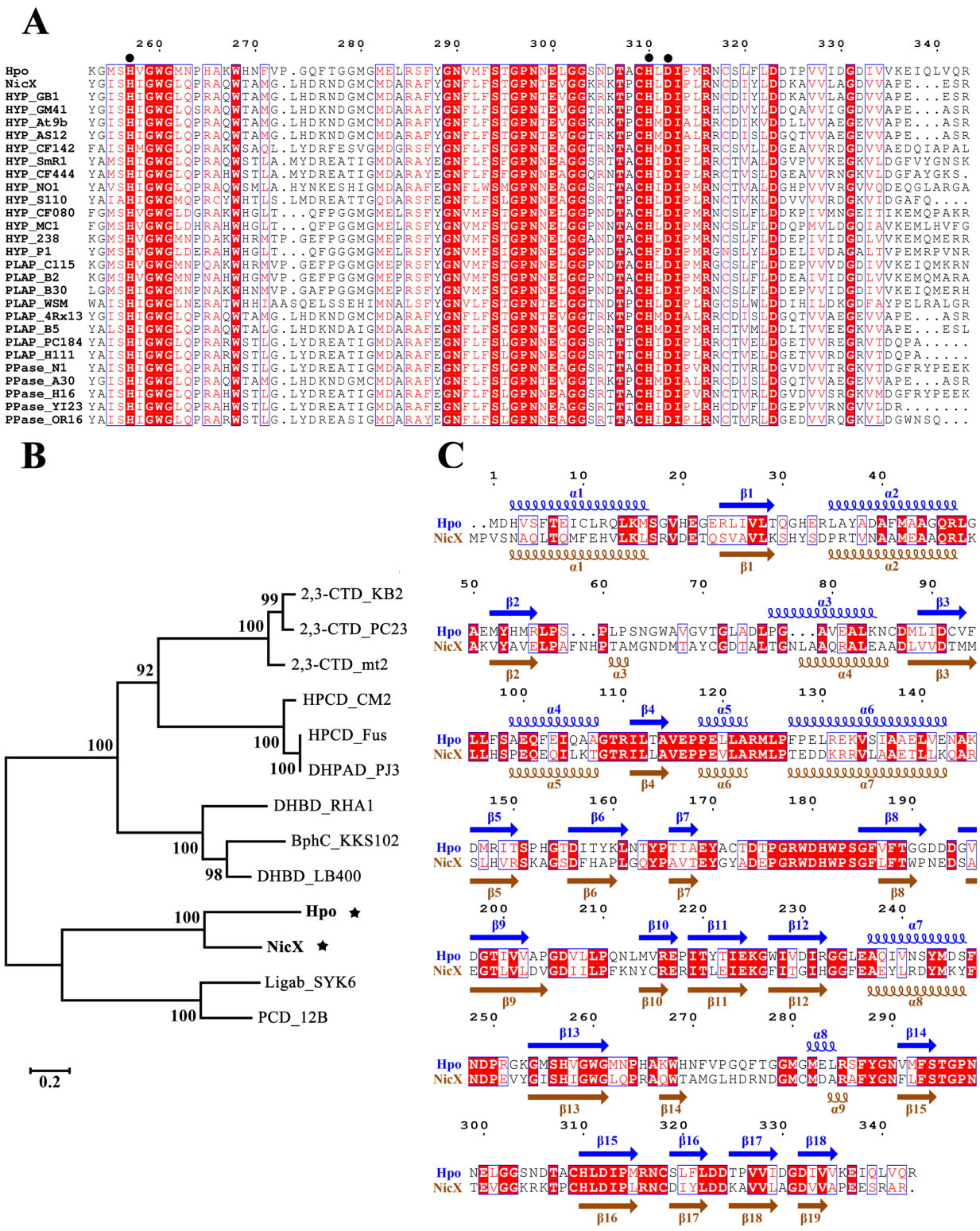

Figure 3 | Amino acid sequence alignment analysis of Hpo. Details of all sequences are included in supplementary information. The sequence alignments were performed with CLUSTAL W. The same residues are highlighted in red and the highly conserved residues are colored in red. (A) Partial sequence alignment of various proteins homologous to Hpo. The probable iron(II) binding sites are indicated by the black circles. The abbreviations of proteins are listed as follows: HYP, hypothetical protein; PLAP, predicted LAP; PPase, predicted M29 family peptidase. (B) Phylogenetic analysis of non-heme iron(II) ring-cleavage dioxygenase. The phylogenetic tree was constructed with the neighbor joining method using MEGA 4.1. Hpo and NicX are indicated by black stars. The abbreviations of dioxygenases are listed as follows: 2,3-CTD, catechol 2,3-dioxygenase; HPCD, homoprotocatechuate 2,3-dioxygenase; DHPAD, 3,4-dihydroxyphenylacetate 2,3-dioxygenase; DHBD, 2,3-dihydroxybiphenyl dioxygenase; BphC, 2,3-dihydroxybiphenyl-1,2-dioxygenase; Ligab, protocatechuate 4,5-dioxygenase; PCD, protocatechuate 4,5-dioxygenase. (C) Secondary structure predictions of Hpo and NicX. The secondary structures were predicted by PSIPRED v3.3 on the *PSIPRED* server (http://bioinf.cs.ucl.ac.uk/psipred.html)[32]. The blue and orange shapes indicate the secondary structure of Hpo and NicX, respectively: helix, α-helix; arrows, β-strand.

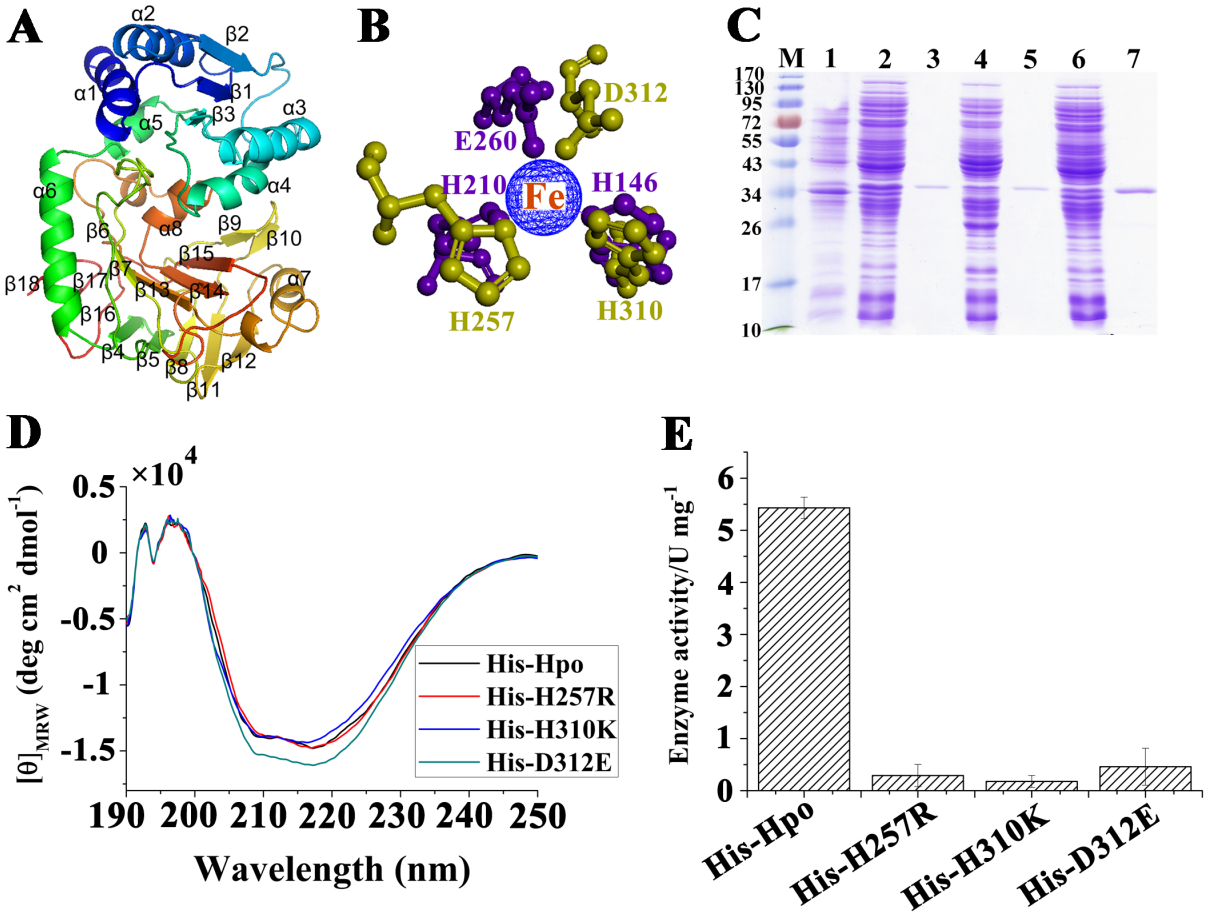

Figure 4 | Predicted three-dimensional model of Hpo and directed mutagenesis of supposed iron(II) binding sites. (A) Predicted three-dimensional structural model of Hpo. (B) Comparison of the iron(II) binding sites. Purple residues, the iron(II) binding sites of BphC from *Bhurkholderia xenovorans* LB400 (PDB_ID, 1HAN); yellow residues, the predicted iron(II) binding sites of Hpo. (C) SDS-PAGE analysis of purified His-H257R, His-H310K and His-D312E variant proteins; M, marker proteins; 1, cell-free extracts of induced *E. coli* BL21(DE3) without plasmid; 2, 4 and 6 cell-free extracts of induced *E. coli* BL21(DE3) harboring plasmid pET28a-*hisH257R*, pET28a-*hisH310K*, and pET28a-*hisD312E*; 3, 5 and 7, purified His-H257R, His-H310K and His-D312E variants. (D) Circular dichroism spectra of His-Hpo, His-H257R, His-H310K and His-D312E. (E) Enzyme activity comparison of His-Hpo and the His-H257R, His-H310K and His-D312E variant proteins; each error bar represents standard deviation of three independent experiments.

should answer these questions. This work has provided basic knowledge that can be used for the analysis of nicotine metabolism in bacteria.

In summary, Hpo is the second member of a new iron(II)-dependent ring-cleavage dioxygenase family, which works with an independent *N*-formylamide deformylase Nfo to catalyze the transformation of 2,5-DHP to maleamate. This study provides a better understanding of the catabolism of 2,5-DHP.

Methods

Materials. L-(-)-Nicotine (≥ 99% purity) was obtained from Fluka Chemie GmbH (Buchs Corp., Buchs, Switzerland). LAP and maleamic acid were from Sigma–Aldrich (Sigma–Aldrich Chemie GmbH, Buchs, SG, Switzerland). Fumaramic acid was made by enzymatic hydrolysis of NFF and characterized by its UV spectrum[19,22]. 2,5-DHP was purchased from SynChem OHG (Kassel Corp., Kassel, Germany). $^{18}O_2$ and $H_2{}^{18}O$ were obtained from the Shanghai Research Institute of Chemical Industry. NFM used as standard was synthesized by the second method described by Behrman et al.[22]. NFF was made as previously reported but note that these papers refer to the product as NFM[10,18]. Behrman described further information on this synthesis in 1976[19]. The MutantBest Kit was purchased from TaKaRa Biotechnology (China). Q Sepharose XL, Source 30Q, Mono Q 5/50 GL, 5 ml HisTrap FF, and 5 ml HiTrap desalting columns were from GE Healthcare (Uppsala, Sweden).

Strains, media and culture conditions. *E. coli* DH5α was grown at 37°C and 220 rpm in lysogenic broth (LB) medium containing the appropriate antibiotics. *E. coli* BL21(DE3) was cultured at appropriate induction expressing conditions in LB medium with 50 μg ml^{-1} kanamycin. *P. putida* S16 was cultured at 30°C in nicotine medium as previously described[2].

Gene isolation, site-directed mutagenesis and plasmid constructions. DNA was isolated, manipulated and transformed according to standard protocols[27]. All primers are listed in Table 2. The *hpo* gene was PCR amplified from the genome DNA of strain S16 using primers hishpo-f/hishpo-r or hpo-f/hpo-r. The variants of *hpoH257R*, *hpoH310K* and *hpoD312E* were acquired by TaKaRa MutantBest Kit according to the manufacturer's instructions. All the products were digested with NcoI and XhoI and cloned into pET28a, then transformed into *E. coli* DH5α or *E. coli* BL21(DE3). The *nicX* gene was PCR amplified from the genome DNA of *P. putida* KT2440 using primers nicX-f/nicX-r, digested with NdeI and HindIII, cloned into pET24a, then transformed into *E. coli* DH5α and *E. coli* BL21(DE3).

Activity analyses of proteins. 2,5-DHP dioxygenase activity was assayed by detecting the absorption of 2,5-DHP at 320 nm (ε_{320} = 5,200 cm^{-1} M^{-1}) with a UV-visible 2550 spectrophotometer (Shimadzu, Japan) at 20°C[17]. The reaction system used 1 ml of 20 mM Tris-HCl buffer (pH 7.5) containing 0.2 mM 2,5-DHP, 0.025 mM Fe^{2+} and 9.6 mg l^{-1} protein. For potential substrates, the oxygen consumption of the reaction was calculated by using a micro-respiration system (Unisense, Denmark), and the substrates decrease was monitored by HPLC. At 20°C, one unit of Hpo in 20 mM Tris-HCl buffer (pH 7.5) catalyzes the oxidation of 1 μmol of 2,5-DHP in 1 min.

LAP activity was assayed by determining the generation of *p*-nitroaniline at 405 nm (ε_{405} = 9,920 cm^{-1} M^{-1}) utilizing L-Leu-*p*-nitroaniline as substrate[28]. One unit of enzyme catalyzes the production of 1 μmol of *p*- nitroaniline in 1 min. The reaction mixture was 5 mM L-Leu-*p*-nitroaniline, 0.025 mM metal ion, and 9.6 mg l^{-1} enzyme in 1 ml of 20 mM Tris-HCl buffer (pH 7.5). LAP was used as the positive control.

Deformylase activity was measured directly by following the disappearance of NFM or NFF by mass spectrometry or, more easily, by monitoring the decrease in absorbance at 290 nm attendant upon formation of the corresponding amide[19]. ε_{290} is 185 cm^{-1} M^{-1} for NFM, 475 cm^{-1} M^{-1} for NFF, 48 cm^{-1} M^{-1} for maleamic acid and 121 cm^{-1} M^{-1} for fumaramic acid. For the mass spectrometric assay, 1 ml of 20 mM

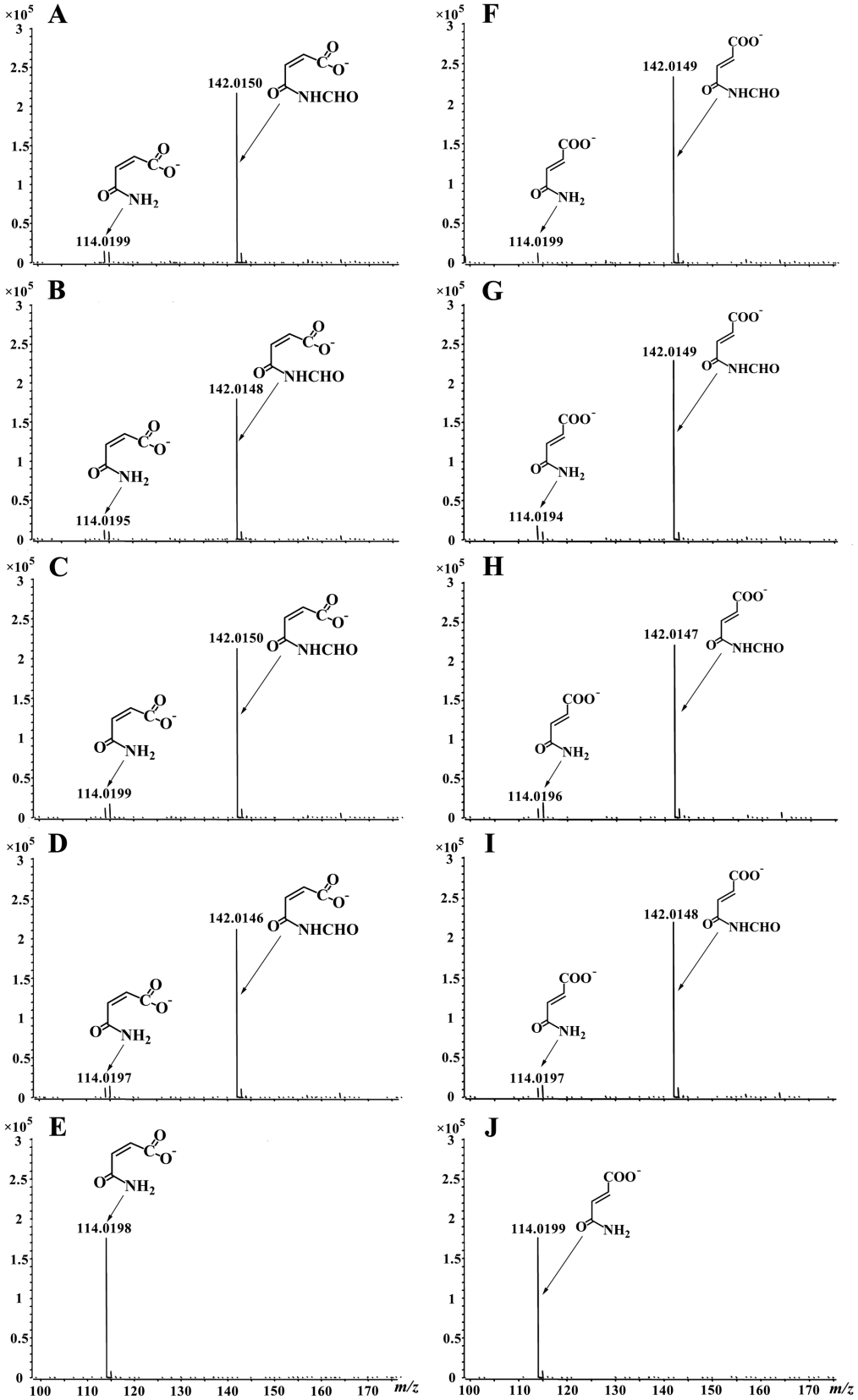

Figure 5 | Mass spectra of reaction solutions using NFM or NFF as substrate. (A) Initial sample of 0.1 mM NFM. (B) 0.1 mM NFM incubated at room temperature for 15 min. (C) 0.1 mM NFM incubated with 9.6 mg l^{-1} Hpo and 0.025 mM Fe^{2+} at room temperature for 15 min. (D) 0.1 mM NFM incubated with 9.6 mg l^{-1} NicX and 0.025 mM Fe^{2+} at room temperature for 15 min. (E) 0.1 mM NFM incubated with 9.6 mg l^{-1} Nfo at room temperature for 15 min. (F) Initial sample of 0.1 mM NFF. (G) 0.1 mM NFF incubated at room temperature for 15 min. (H) 0.1 mM NFF incubated with 1 g l^{-1} Hpo and 0.025 mM Fe^{2+} at room temperature for 15 min. (I) 0.1 mM NFF incubated with 1 g l^{-1} NicX and 0.025 mM Fe^{2+} at room temperature for 15 min. (J) 0.1 mM NFF incubated with 1 g l^{-1} Nfo at room temperature for 15 min.

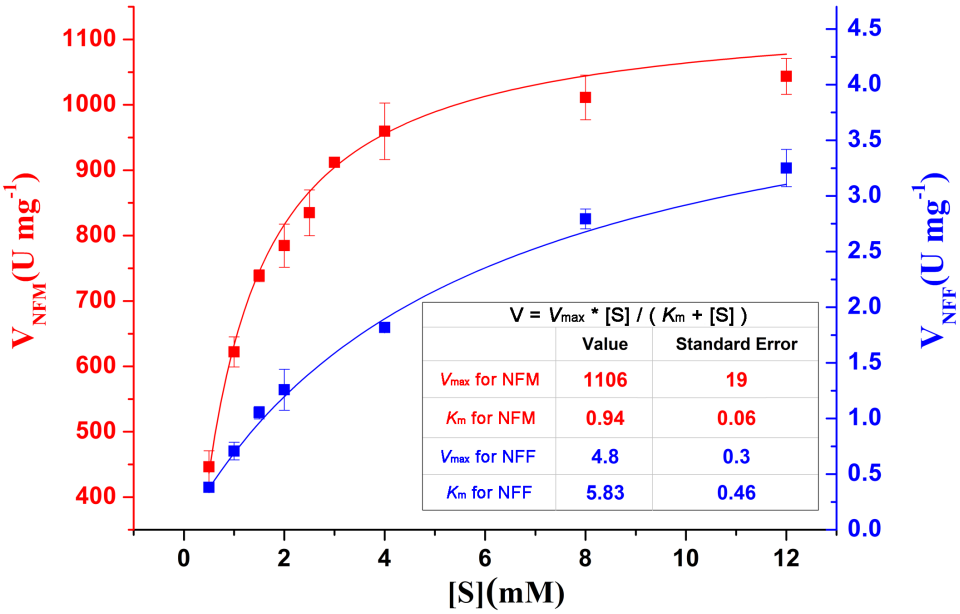

Figure 6 | Kinetic studies of Nfo for NFM and NFF. The experiments were performed in 1 ml of 20 mM Na_2HPO_4-NaH_2PO_4 buffer (pH 6.7) at 25°C. Red line, fitted Michaelis-Menten curve of Nfo for NFM; blue line, fitted Michaelis-Menten curve of Nfo for NFF; each error bar represents standard deviation of three independent experiments. The inset table shows the Michaelis-Menten equation and the fitted parameters.

Tris-HCl buffer (pH 7) containing 0.1 mM substrate, 0.025 mM Fe^{2+}, and appropriate concentrations of enzymes (9.6 mg l^{-1} for NFM and 1 g l^{-1} for NFF) were incubated at room temperature for 15 min. The UV assay used 1 ml of 20 mM Na_2HPO_4-NaH_2PO_4 buffer (pH 6.7) containing 1 mM substrate and appropriate concentrations of Nfo (2 mg l^{-1} for NFM and 0.1 g l^{-1} for NFF) that were incubated at 20°C. Because there is about 1% (w/w) sodium iodate in the NFM sample, more sodium iodate (1%, w/w) was added to the NFM catalyzed system to see if iodate affects the activity of Nfo; it does not. All these experiments were performed in a dark room. At 25°C, one unit of Nfo in 20 mM Na_2HPO_4-NaH_2PO_4 buffer (pH 6.7) can catalyze the hydrolysis of 1 μmol of substrate in 1 min.

Purification of proteins. *E. coli* BL21(DE3) strains carrying the recombinant plasmids were cultured to OD_{600} 0.6 ~ 0.8 at 37°C, 220 rpm. The cells were induced by addition of isopropyl thiogalactoside (IPTG) to a final concentration of 0.1 mM, followed by growth at 30°C for 10 h. All the steps of chromatography were performed by an ÄKTA purifier (GE Healthcare Bio-Sciences, Sweden). Ni binding buffer contained 50 mM NaH_2PO_4, 300 mM NaCl and 10 mM imidazole (pH 8.0), while Ni elution buffer contained 50 mM NaH_2PO_4, 300 mM NaCl and 250 mM imidazole (pH 8.0). The low salt buffer was 20 mM Tris-HCl (pH 7.5) and the high salt buffer was 20 mM Tris-HCl plus 1 M NaCl (pH 7.5). One mM DTT was added to all the buffers before use.

The cells expressing His_6-tagged proteins were resuspended in Ni binding buffer (OD_{600} 50) after centrifugation (5,000 × *g*, 10 min) and sonicated (150 W, on ice for 10 min). After centrifugation (12,000 × *g*, 20 min), the supernatant was loaded onto a 5 ml HisTrap FF column pre-equilibrated with Ni binding buffer, and the column was washed with 100 mM imidazole. His_6-tagged proteins were eluted by 150 mM imidazole, and 250 mM imidazole was applied to clear the column. Concentration of the proteins was performed by ultrafiltration (Millipore Corporation, USA), and the concentrates were desalted through a 5 ml HiTrap desalting columns to change the buffer to low salt buffer. The purified proteins were stored at −80°C.

The non-His_6-tagged protein (Hpo) was purified as follows. The cell-free supernatant obtained after sonication was applied to a 1.6 × 10-cm Q Sepharose XL column pre-equilibrated with low salt buffer, and eluted with a step gradient of 0, 0.6 M and 1 M NaCl in 20 mM Tris-HCl buffer (pH 7.5). Hpo eluting with 0.6 M NaCl was pooled, concentrated and desalted. The Hpo solution from the last step was loaded onto a Source 30Q column (1.6 × 10-cm) equilibrated with low salt buffer, and the column was washed with a step gradient of 0.35 M, 0.45 M and 1 M NaCl. The active fractions containing 0.45 M NaCl were concentrated and desalted. Finally, the enzyme solution was applied to a 0.5 × 5-cm Mono Q column pre-equilibrated with 20 mM Tris-HCl buffer (pH 7.5). The column was washed with 0.45 M NaCl, and Hpo was eluted with 0.55 M NaCl. The purified Hpo solution was desalted to change the buffer to 20 mM Tris-HCl (pH 7.5) and stored at −80°C until further use. All proteins were quantified by the Bradford method using bovine serum albumin as standard[29].

Electrophoresis. Electrophoresis was performed using a 1% agarose gel[30]. SDS-PAGE and native-PAGE were carried out as previously described[31].

Size-exclusion chromatography analysis. Size-exclusion chromatography analysis was performed as described by Jiménez et al.[26]. The Superdex 200 10/300 GL Tricorn column (GE Healthcare) was equilibrated with 20 mM Tris-HCl (pH 7.5) containing 1 mM DTT. Thyroglobulin (669 kDa), apoferritin (443 kDa), aldolase (158 kDa), conalbumin (75 kDa) and ovalbumin (44 kDa) in the same buffer were used to calibrate the column. The K_{av} values of the proteins were calculated according to the formula $K_{av} = (V_e - V_0)/(V_t - V_0)$ (V_e: elution volume, V_0: void volume, V_t: total volume of the column). The size of Hpo was determined by its K_{av} value three times according to a fitted standard curve of a base-10 logarithm of the molecular weight (MW) of the standard proteins *versus* their K_{av} values.

^{18}O labeling. $H_2{}^{18}O$ (≥ 98% purity) and $^{18}O_2$ (≥ 98% purity) were used to determine the source of the oxygen atoms in NFM. The $H_2{}^{18}O$ labeling reaction was 1 ml of $H_2{}^{18}O$ containing 1 mM 2,5-DHP, 0.025 mM Fe^{2+} and 10 μg ml^{-1} Hpo, incubated at 25°C for 5 min. The $^{18}O_2$ labeling reaction was performed in a rubber sealed bottle attached to an anaerobic workstation (model AW200SG; Electrotek Ltd, UK) filled with a gas mixture of 10% H_2, 10% CO_2 and 80% N_2. One ml of H_2O containing 1 mM 2,5-DHP and 0.025 mM Fe^{2+} was injected into the bottle, air in the bottle was replaced by the continuous gas mixture, $^{18}O_2$ was injected, and 10 μg Hpo was added to the bottle, with the mixture incubated at 25°C for 5 min. Another reaction containing 1 ml H_2O, 1 mM 2,5-DHP, 0.025 mM Fe^{2+} and 10 μg ml^{-1} Hpo in air was used as a control. The supernatants were directly analyzed by LC-MS after ethanol precipitation and centrifugation (12,000 × *g*, 2 min).

Analytical techniques. 2,5-DHP, 2,5-DHP analogues, NFM and NFF were monitored at 254 nm by HPLC using an Agilent eclipse XDB C-18 (5 μm, 0.46 × 15 cm). The mobile phase was a mixture (90 : 10, vol/vol) of H_2O containing 0.1% HCOOH and methanol containing 0.1% HCOOH, the flow rate was 0.2 ml min^{-1} and the column temperature was 30°C. Mass spectra of 2,5-DHP, NFM and maleamic acid were acquired using an Agilent 1290 (ultra performance liquid chromatography, UPLC) coupling with an Agilent 6230 electrospray ionization time-of-flight mass spectrometry (ESI-TOF-MS). The reaction mixtures were precipitated with ethanol and centrifuged (12,000 × *g*, 2 min). The supernatants were analyzed by direct-insertion mass spectra in the negative-ion turbo ion spray ionization mode. The theoretical *m/z* values of 2,5-DHP, NFM, NFM with two ^{18}O atoms, and maleamic acid were 110.0248, 142.0146, 146.0231 and 114.0197, respectively.

Structure predicting. The secondary structures of the proteins were predicted by PSIPRED v3.3 on *PSIPRED* server (http://bioinf.cs.ucl.ac.uk/psipred.html)[32]. The method of three-dimensional modeling was as previously described[31]; templates for further structure prediction of Hpo are listed in Table S1. The iron(II) binding sites of BphC (PDB_ID, 1HAN), which is a extradiol dioxygenase from *Bhurkholderia xenovorans* LB400, was used to compare with the predicted iron(II) binding sites of Hpo[33]. The comparison was illustrated by Discovery Studio 3.5 (Accelrys, San Diego, CA). The sequence of the Nfo protein was searched in the protein data bank by the PSI-BLAST program on the NCBI web site. Among all the similar sequences revealed by BLAST program, the epoxide hydrolase from *Agrobacterium radiobacter* AD1 (PDB_ID: 1EHY) shows the highest sequence identity of 36% and a very low E value as well[34]. Thus, its crystal structure was used as the template to construct the homology model of Nfo. Ten homology models were constructed by the MODELLER package. The structure with the best score is displayed (Fig. S3).

Secondary structure analysis by circular dichroism spectra. The circular dichroism spectra of His-Hpo and the variant proteins were obtained by JASCO J-815 at 25°C. The samples were 0.1 mg ml^{-1} His-Hpo, His-H257R, His-H310K and His-D312E in 20 mM NaH_2PO_4-Na_2HPO_4 buffer (pH 7.5), respectively. The measurement range was 190 nm – 250 nm; the cell length was 1.0 mm; 10 spectra were accumulated for each run. According to the circular dichroism spectra, the secondary structure compositions of the proteins were calculated by using the software CDPro (CONTINLL, reference protein set: SMP50).

1. Padoley, K. V., Mudliar, S. N. & Pandey, R. A. Heterocyclic nitrogenous pollutants in the environment and their treatment options–an overview. *Bioresource Technol.* **99**, 4029–4043 (2008).
2. Wang, S. N. *et al.* Biodegradation and detoxification of nicotine in tobacco solid waste by a *Pseudomonas* sp. *Biotechnol. Lett.* **26**, 1493–1496 (2004).
3. Sims, G. K., O'Loughlin, E. J. & Crawford, R. L. Degradation of pyridines in the environment. *Crit. Rev. Environ. Control* **19**, 309–340 (1989).
4. Richards, D. J. & Shieh, W. K. Biological fate of organic priority pollutants in the aquatic environment. *Water Res.* **20**, 1077–1090 (1986).
5. Rogers, J. E., Riley, R. G., Li, S. W., O'Malley, M. L. & Thomas, B. L. Microbial transformation of alkylpyridines in groundwater. *Water Air Soil Pollut.* **24**, 443–454 (1985).
6. Kuhn, E. P. & Suflita, J. M. Microbial degradation of nitrogen, oxygen and sulfur heterocyclic compounds under anaerobic conditions: studies with aquifer samples. *Environ. Toxicol. Chem.* **8**, 1149–1158 (1989).
7. Kaiser, J. P., Feng, Y. & Bollag, J. M. Microbial metabolism of pyridine, quinoline, acridine, and their derivatives under aerobic and anaerobic conditions. *Microbiol. Rev.* **60**, 483–498 (1996).
8. Orpin, C. G., Knight, M. & Evans, W. C. The bacterial oxidation of picolinamide, a photolytic product of diquat. *Biochem. J.* **127**, 819–831 (1972).
9. Shukla, O. P. & Kaul, S. M. Microbiological transformation of pyridine *N*-oxide and pyridine by *Nocardia* sp. *Can. J. Microbiol.* **32**, 330–341 (1986).
10. Tang, H. Z. *et al.* Genomic analysis of *Pseudomonas putida*: genes in a genome island are crucial for nicotine degradation. *Sci. Rep.* **2**, 377, doi:10.1038/srep00377 (2012).
11. Tang, H. Z. *et al.* Systematic unraveling of the unsolved pathway of nicotine degradation in *Pseudomonas*. *PLoS Genet.* **9**, e1003923, doi:10.1371/journal.pgen.1003923 (2013).
12. Cain, R. B., Houghton, C. & Wright, K. A. Microbial metabolism of the pyridine ring: metabolism of 2-and 3-hydroxypyridines by the maleamate pathway in *Achromobacter* sp. *Biochem. J.* **140**, 293–300 (1974).
13. Jiménez, J. I. *et al.* Deciphering the genetic determinants for aerobic nicotinic acid degradation: the *nic* cluster from *Pseudomonas putida* KT2440. *Proc. Natl. Acad. Sci. USA* **105**, 11329–11334 (2008).
14. Kim, S. G. & Novak, R. F. Role of P450IIE1 in the metabolism of 3-hydroxypyridine, a constituent of tobacco smoke: redox cycling and DNA strand scission by the metabolite 2,5-dihydroxypyridine. *Cancer Res.* **50**, 5333–5339 (1990).
15. Behrman, E. J. & Stanier, R. Y. The bacterial oxidation of nicotinic acid. *J. Biol. Chem.* **228**, 923–945 (1957).
16. Stanier, R. Y., Palleroni, N. J. & Doudoroff, M. The aerobic *Pseudomonads*: a taxonomic study. *J. Gen. Microbiol.* **43**, 159–271 (1966).
17. Gauthier, J. J. & Rittenberg, S. C. The metabolism of nicotinic acid. I. purification and properties of 2,5-dihydroxypyridine oxygenase from *Pseudomonas putida* N-9. *J. Biol. Chem.* **246**, 3737–3742 (1971).
18. Gauthier, J. J. & Rittenberg, S. C. The metabolism of nicotinic acid. II. 2,5-dihydroxypyridine oxidation, product formation, and oxygen 18 incorporation. *J. Biol. Chem.* **246**, 3743–3748 (1971).
19. Behrman, E. J. The bacterial oxidation of nicotinic acid. *N*-formylmaleamic and *N*-formylfumaramic acids. *Arch. Microbiol.* **110**, 87–90 (1976).
20. Behrman, E. J. *N*-formylmaleamic acid: an intermediate in nicotinic acid metabolism. *Proc. Natl. Acad. Sci. USA* **105**, E88 (2008).
21. Jiménez, J. I. *et al.* Reply to Behrman:"*N*-Formylmaleamic acid: an intermediate in nicotinic acid metabolism". *Proc. Natl. Acad. Sci. USA* **105**, E89 (2008).
22. Behrman, E. J. & Hillenbrand, E. L. Synthesis of *N*-formylmaleamic acid and some related *N*-formylamides. *J. Chem. Res.* 170–172 (2008).
23. Koehntop, K. D., Emerson, J. P. & Que, L. The 2-His-1-carboxylate facial triad: a versatile platform for dioxygen activation by mononuclear non-heme iron(II) enzymes. *J. Biol. Inorg. Chem.* **10**, 87–93 (2005).
24. Odintsov, S. G., Sabala, I., Bourenkov, G., Rybin, V. & Bochtler, M. *Staphylococcus aureus* aminopeptidase S is a founding member of a new peptidase clan. *J. Biol. Chem.* **280**, 27792–27799 (2005).
25. Holmquist, M. Alpha/beta-hydrolase fold enzymes: structures, functions and mechanisms. *Curr. Protein Pept. Sci.* **1**, 209–235 (2000).
26. Jiménez, J. I., Acebrón, I., García, J. L., Díaz, E. & Mancheño, J. M. A preliminary crystallographic study of recombinant NicX, an Fe(2+)-dependent 2,5-dihydroxypyridine dioxygenase from *Pseudomonas putida* KT2440. *Acta Crystallogr. Sect. F Struct. Biol. Cryst. Commun.* **66**, 549–553 (2010).
27. Sambrook, J. & Russell, D. W. *Molecular cloning: a laboratory manual.* 3rd edn, Vol. **1**, (Cold Spring Harbor Laboratory press, 2001).
28. Hattori, A. *et al.* Characterization of recombinant human adipocyte-derived leucine aminopeptidase expressed in Chinese hamster ovary cells. *J. Biochem.* **128**, 755–762 (2000).
29. Bradford, M. M. A rapid and sensitive method for the quantitation of microgram quantities of protein utilizing the principle of protein-dye binding. *Anal. Biochem.* **72**, 248–254 (1976).
30. Southern, E. M. Detection of specific sequences among DNA fragments separated by gel electrophoresis. *J. Mol. Biol.* **98**, 503–517 (1975).
31. Tang, H. Z. *et al.* A novel NADH-dependent and FAD-containing hydroxylase is crucial for nicotine degradation by *Pseudomonas putida*. *J. Biol. Chem.* **286**, 39179–39187 (2011).
32. Bryson, K. *et al.* Protein structure prediction servers at University College London. *Nucleic Acids Res.* **33**, W36–38 (2005).
33. Han, S., Eltis, L. D., Timmis, K. N., Muchmore, S. W. & Bolin, J. T. Crystal structure of the biphenyl-cleaving extradiol dioxygenase from a PCB-degrading pseudomonad. *Science* **270**, 976–980 (1995).
34. Nardini, M. *et al.* The x-ray structure of epoxide hydrolase from *Agrobacterium radiobacter* AD1. An enzyme to detoxify harmful epoxides. *J. Biol. Chem.* **274**, 14579–14586 (1999).

Acknowledgments

This work was supported by the grants from the Chinese National Natural Science Foundation (31230002 and 31121064). We also acknowledge the Shanghai Rising-Star Program (13QA1401700) and the Chen Xing Project of Shanghai Jiao Tong University. The authors would like to acknowledge Ben Ma, Tingwen Bao, Jun Hao and Rong Zou (Shanghai Jiao Tong University) for their technical assistance on the scientific projects. We thank Prof. Robert P. Hausinger (Michigan State University) for very helpful and scientific comments on the manuscript. We also thank Dr. Dake Zhang (Beijing Institute of Genomics) and Ruoxu Gu (Shanghai Jiao Tong University) for the kind help in three-dimensional structure predictions of Hpo and Nfo.

Author contributions

P.X., Y.Y., H.T. and E.J.B. conceived and designed the project and experiments. E.J.B. synthesized the NFM. Y.Y., H.R., H.Y., L.W. and W.Z. performed the experiments. Y.Y., H.T., E.J.B. and P.X. analyzed the data and wrote the paper. All authors reviewed the paper.

Additional information

Supplementary information accompanies this paper at http://www.nature.com/scientificreports

Competing financial interests: The authors declare no competing financial interests.

How to cite this article: Yao, Y.X. *et al.* Iron(II)-dependent dioxygenase and *N*-formylamide deformylase catalyze the reactions from 5-hydroxy-2-pyridone to maleamate. *Sci. Rep.* **3**, 3235; DOI:10.1038/srep03235 (2013).